Catalysis Today 175 (2011) 171–176

Contents lists available at ScienceDirect

Catalysis Today

journal homepage: www.elsevier.com/locate/cattod

Low-temperature selective catalytic reduction of NO with NH_3 over monolith catalyst of MnO_x/CeO_2–ZrO_2–Al_2O_3

Qiulin Zhang, Chuntian Qiu, Haidi Xu, Tao Lin*, Zhien Lin, Maochu Gong, Yaoqiang Chen*

Key Laboratory of Green Chemistry and Technology of the Ministry of Education, College of chemistry, Sichuan University, Chengdu 610064, PR China

ARTICLE INFO

Article history:
Received 14 October 2010
Received in revised form 4 May 2011
Accepted 16 May 2011
Available online 12 June 2011

Keywords:
SCR
Low temperature
NO
Monolith catalyst
Manganese

ABSTRACT

MnO_x/CeO_2–ZrO_2–Al_2O_3 (MnO_x/CZA) catalysts with different amounts of manganese loading were prepared by incipient wetness impregnation method for selective catalytic reduction (SCR) of NO with NH_3 at low temperature. The catalysts were characterized by N_2 adsorption–desorption measurement, XRD, XPS, and H_2-TPR. Catalytic activity tests reveal that the MnO_x/CZA catalyst with 10% manganese loading has the best catalytic activity, almost 90% NO is translated to N_2 in the temperature range of 143–300 °C. The highly dispersed MnO_x species, the good oxidation activity of NO to NO_2, the existent synergistic effect between the manganese and cerium oxides, and the various oxidation states of manganese oxides may be the main reasons for the best SCR activity. In addition, the SCR activity is slightly influenced in the presence of SO_2 and H_2O, while such effect is restorable after heating treatment.

1. Introduction

Nitrogen oxides from the combustion of fossil fuels are the main source of air pollution, and they contribute to acid rain, photochemical smog and ozone depletion. Currently, selective catalytic reduction (SCR) of NO_x with NH_3 in the presence of excessive O_2 has been widely applied to reduce the emission of nitrogen oxides for its low cost and high efficiency [1]. As the most prevalent commercial catalyst, V_2O_5–WO_3/TiO_2 exhibits high activity. But this catalyst is only active in a narrow temperature window of 300–400 °C [2,3]. Consequently, a highly efficient low-temperature SCR catalyst is often desired to avoid the reheating of flue gas and the deactivation caused by SO_2 and dust presented in the flue gas of stationary source. This catalyst can be located downstream of the equipment of desulfurizer and particle removal without preheating the flue gas.

In recent years, the Mn-based catalysts have been found to be highly effective for low temperature SCR of NO with NH_3, and TiO_2, Al_2O_3, SiO_2 and active carbon have been widely used as the support of the low temperature SCR catalyst [4–10]. In some studies, CeO_2 has been used to promote the SCR activity due to its ability of creating surface and bulk oxygen vacancies by generation Ce^{3+}/Ce^{4+} redox couples. The surface and bulk oxygen vacancies can promote the oxidization of NO to NO_2, which will increase the catalytic activity for SCR of NO with NH_3 [11,12]. However, the specific surface area of CeO_2 is not large enough, and its ability of creating surface and bulk oxygen vacancies needs to be improved. As a new generation oxygen-storage material, CeO_2–ZrO_2–Al_2O_3 (CZA) is widely used in three-way catalysts [13–15]. CZA has potential application in NH_3-SCR catalyst for its high thermal stability, high surface area and fine ability of creating surface and bulk oxygen vacancies. It is well-known that the monolith catalyst is more representative in catalysis application for its low pressure drop, short diffusion distances and large geometric surface area [16]. In this study, monolith MnO_x/CZA catalysts with different manganese loadings were prepared and they were characterized by N_2 adsorption–desorption measurement, XRD, XPS and H_2-TPR.

2. Experimental

2.1. Preparation of supports and catalysts

CeO_2–ZrO_2–Al_2O_3 (CZA) and TiO_2 were prepared by co-precipitation method. To prepare CZA support, a mixture of $Ce(NO_3)_3{\cdot}6H_2O$, $ZrOCO_3{\cdot}nH_2O$, and $Al(NO_3)_3{\cdot}9H_2O$ in a molar ratio of 3:3:4 was dissolved in distilled water. The mixed aqueous solution of ammonia and $(NH_4)_2CO_3$ was used as the precipitator and was added dropwise to the metal salt solution. The resulting precipitates were aged, filtered, washed, and dried at 110 °C overnight, and then they were calcined at 600 °C for 3 h. TiO_2 was prepared under the similar conditions as used for CZA support, except that $TiOSO_4{\cdot}2H_2O$ was used as the metal salt and it was calcined at 500 °C for 3 h.

* Corresponding authors. Tel.: +86 28 85418451; fax: +86 28 85418451.
E-mail addresses: lintaochem@scu.edu.cn (T. Lin), nic7501@scu.edu.cn (Y. Chen).

0920-5861/$ – see front matter © 2011 Elsevier B.V. All rights reserved.
doi:10.1016/j.cattod.2011.05.009

MnO_x/CZA catalysts with different manganese loadings were prepared by impregnating the CeO_2–ZrO_2–Al_2O_3 powder with $Mn(CH_3COO)_2{\cdot}2H_2O$ aqueous solution. Then the samples were dried at 105 °C overnight and calcined at 500 °C for 3 h. The resulting powders were subsequently coated on honeycomb cordierites (2.5 cm^3, Yi Xing, China) and calcined at 500 °C for 3 h in air. The washcoat loading was about 180 g/L. These MnO_x/CZA catalysts containing 5 wt.%, 10 wt.%, 15 wt.%, 20 wt.% and 30 wt.% manganese are referred as Cat-A, Cat-B, Cat-C, Cat-D and Cat-E.

MnO_x/TiO_2 catalyst with 10% manganese loading (denoted as Cat-O) was prepared under the similar conditions as used for MnO_x/CZA catalysts. The pure MnO_x was prepared by calcination of $Mn(CH_3COO)_2{\cdot}2H_2O$ at 500 °C for 3 h and then coated on honeycomb cordierites and calcined at 500 °C for 3 h in the air.

2.2. Characterization of the catalysts

BET surface area measurement was carried out on QUADRASORB *SI* automatic surface analyzer (Quantachrome Corporation). The samples were evacuated for 3 h at 300 °C, and then cooled to −196 °C using liquid N_2 at which point N_2 adsorption was measured.

Powder X-ray diffraction (XRD) data were collected on Rigaku D/MAX-rA diffractometer with Cu radiation (λ = 0.15406 nm). The X-ray tube was operated at 45 kV and 25 mA. The samples were investigated in the 2θ range of 10–90° at a scanning speed of 0.03° S^{-1}.

The H_2-temperature programmed reduction (H_2-TPR) was carried out in a quartz U-tube, and 100 mg sample was employed for each measurement. The sample was first pre-treated in N_2 (30 ml min^{-1}) at 450 °C for 1 h and then cooled to room temperature. After that, a flowing H_2 (5% in N_2, 30 ml min^{-1}) was switched on with a linear heating rate of 8 °C min^{-1}. A thermal conductivity cell was used to detect the consumption of H_2.

XPS experiments were carried out on a spectrometer (XSAM-800, KRATOS Co.) with Al Kα radiation under UHV, The C 1s peak (284.8 eV) was used for the calibration of binding energy values. The pressure in the analytical chamber was about 10^{-9} Pa.

2.3. Catalytic activity measurements

The catalytic activity measurement was carried out in a fixed-bed quartz flow reactor. Reactant gases were regulated by means of mass-flow controllers before entering reactor. The concentration of simulated gases were as follow: 1000 ppm NO, 1000 ppm NH_3, 5% O_2, 10% water vapor (when used), 100 ppm SO_2 (when used), balance Ar, the gas hourly space velocity (GHSV) = 10,000 h^{-1}, the total flow rate was 416 ml min^{-1}. The water vapor was generated by passing Ar flow through a gas-wash device containing de-ionized water. The NO and NO_2 concentrations in the inlet and outlet gases were continually analyzed by a chemiluminescent NO/NO_x analyzer (Model 42i, Thermo Electron Corporation). To avoid the influence caused by the oxidation of ammonia, the outlet stream was passed through an ammonia trap containing phosphoric acid solution before entering the chemiluminescent analyzer. The catalysts were pre-treated in Ar at 500 °C for 1 h before activity test.

The catalytic oxidation activities for NO to NO_2 were also measured. The reaction conditions were as follow: 1000 ppm NO, 5% O_2, balance Ar, GHSV = 10,000 h^{-1}. The conversion of NO to NO_2 was obtained by this equation: Conversion of NO to NO_2 = 100% × ([NO_x]inlet − [NO]outlet)/[NO_x]inlet, where NO_x represents NO + NO_2.

Table 1
BET surface area, pore volume and pore size of CZA and MnO_x/CZA catalysts.

Samples	BET surface area (m^2 g^{-1})	Pore volume (cm^3 g^{-1})	Pore size (nm)
CZA	193	0.317	9.68
Cat-A	137	0.282	9.36
Cat-B	127	0.258	8.88
Cat-C	125	0.231	7.92
Cat-D	116	0.208	7.20
Cat-E	112	0.187	6.88

3. Results and discussion

3.1. Nitrogen adsorption and XRD

The BET surface area, pore volume, and pore size of various samples are summarized in Table 1. From Table 1, we can see that the specific surface area (193 m^2 g^{-1}), pore volume (0.32 cm^3 g^{-1}) and pore size (9.6 nm) of the CZA support are the largest among all of the samples. With the increase of manganese loading, a decrease of BET surface area, pore volume and pore size is observed. This can be easily understood by the fact that the free pore of CZA support is partially occupied by the manganese oxides.

XRD patterns of pure MnO_x and MnO_x/CZA with different manganese content are shown in Fig. 1. The diffraction peaks of pure MnO_x are characteristic of Mn_2O_3, no other manganese oxides diffraction peaks are observed. It is noteworthy that the XRD patterns of MnO_x/CZA catalysts and CZA presented here reveal no visible Al_2O_3 diffraction peaks except for the distinct cubic fluorite-type phase diffraction peaks of $Ce_{0.5}Zr_{0.5}O_2$. Although large amounts of Al_2O_3 (40 wt.%) exist in CZA, not any Al_2O_3 diffraction peaks are observed from XRD patterns. Thus the Al_2O_3 in CZA forms solid solution accompany with $Ce_{0.5}Zr_{0.5}O_2$ solid solution more likely. This result shows that CZA forms homogeneous solid solutions and the Al_2O_3 disperses well in CZA solid solutions. At low manganese loadings (≤10%), no manganese oxide diffraction peaks can be found. This may be due to the highly dispersed manganese oxide on CZA, or the amorphous phase of manganese oxide has formed on the surface of catalyst. As the manganese content increases, the crystal phase of Mn_3O_4 becomes apparent, and the visible crystal phase of Mn_2O_3 is also detected when the manganese loading reaches 30%. From the XRD results, it can be concluded that the manganese oxides disperse well on the MnO_x/CZA with

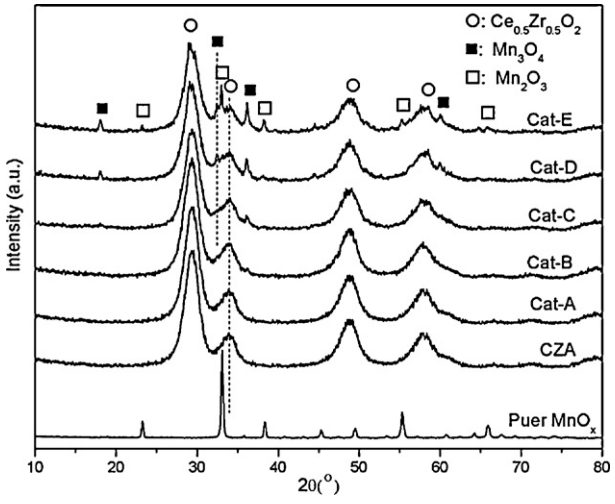

Fig. 1. XRD patterns of MnO_x/CZA catalysts with different manganese loading. Cat-A, Cat-B, Cat-C, Cat-D and Cat-E denote as MnO_x/CZA with 5%, 10%, 15%, 20% and 30% manganese loading, respectively.

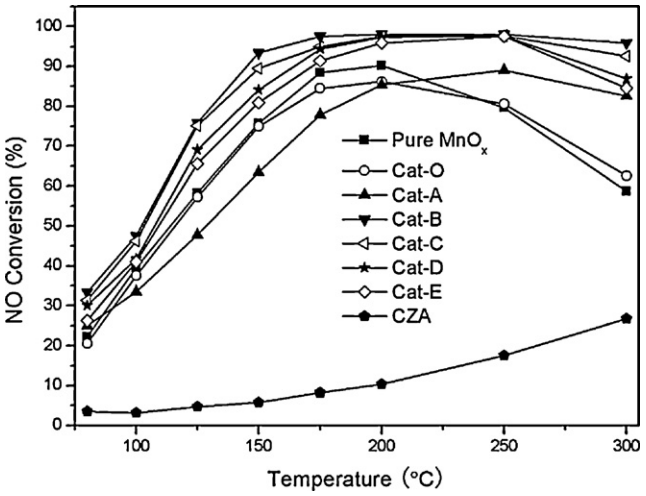

Fig. 2. NO conversion on different catalysts. Reaction conditions: total flow rate: 416 ml min^{-1}, 1000 ppm NO, 1000 ppm NH_3, 5% O_2 and Ar balance, GHSV = 10,000 h^{-1}.

10% manganese content. Otherwise, the strong interaction between MnO_x and CZA induces the translating of Mn_2O_3 oxidation state to various oxidation states of manganese oxides in MnO_x/CZA catalysts.

3.2. Catalytic performance

The catalytic activities of various catalysts for low-temperature SCR at a gases space velocity of 10,000 h^{-1} as a function of reaction temperature are shown in Fig. 2. It can be seen that the highest conversion of NO over the pure MnO_x and Cat-O monolith catalyst is below 85%, and they have a narrow activity temperature window of 160–250 °C (NO conversion > 80%). The CZA exhibits more inferior NO conversion, the highest conversion of NO is only 26.7%, and almost no NO conversion is obtained at low temperature (80–150 °C). In comparison, MnO_x/CZA series catalysts are highly active at low temperature. As shown in Fig. 2, the NO conversion shows an evident upward trend with the increase of manganese loading until the manganese content reaches 10%. After this level, a further increase of manganese loading does not increase the activity. It can be seen that the catalyst with 5% manganese content exhibits inferior SCR activity, which may be caused by the lacking of enough active sites. The catalyst with 10% manganese loading has the lowest light-off temperature (NO conversion is 50%) and the widest activity temperature window. It is light-off at 103 °C, which is much lower than that of other catalysts. In the temperature range of 143–300 °C, almost 90% NO conversion is presented over Cat-B. This is much better than those monolith catalysts reported in Refs. [8,9]. Considering the XRD results, it can be concluded that the finely dispersed manganese oxide on CZA is the main contribution to the SCR activity. With the increase of manganese loading, the highly dispersed MnO_x species may aggregate and the appearance of crystalline manganese oxide decreases the SCR activity.

3.3. The oxidation activity of NO to NO_2

Taking account of NO can be oxidized to NO_2 in the presence of excessive O_2, the conversion of NO to NO_2 in the absence of catalyst was measured with different concentrations of NO. As shown in Fig. 3(a), there are only a few conversions of NO to NO_2 in the absence of catalyst. The lower concentrations of NO exhibit better oxidation activity of NO to NO_2. When the concentrations of NO are 200 ppm, the conversion of NO to NO_2 is the highest, which is 3.8% at 300 °C. The conversions of NO to NO_2 gradually decrease with the increase of NO concentrations. Otherwise, with the increasing of temperature in the range of 80–300 °C, the conversions of NO to NO_2 increase. Thus it can be seen that the oxidation activity of NO to NO_2 is very low in the absence of catalyst.

The conversions of NO to NO_2 as a function of reaction temperature in excess oxygen over MnO_x, Cat-O and Cat-B catalysts are shown in Fig. 3(b). It is obvious that the introduction of the catalyst increases the oxidation activity of NO to NO_2. However, the oxidation activity of NO to NO_2 on MnO_x and Cat-O is still low, especially at lower temperature. At 100 °C, there are only 2.1% and 1.8% conversions over MnO_x and Cat-O, respectively. After MnO_x supporting on CZA oxygen storage material, the NO oxidation activity increases significantly, and the conversion over Cat-B catalyst is 4.6% at 100 °C and 13.3% at 150 °C. It has been established that NO is more readily reduced to N_2 along with portion NO_2 than single NO by ammonia [17,18]. It can be seen from Fig. 3(b), the introduction of CZA oxygen storage material increases the oxidation rate of NO to NO_2, which increases the SCR activity.

3.4. XPS analysis

To understand the surface properties of MnO_x/CZA catalysts, XPS studies were carried out. As shown in Fig. 4 and Table 2, a significant increase in the intensity and sharpening of Mn 2p peaks can be

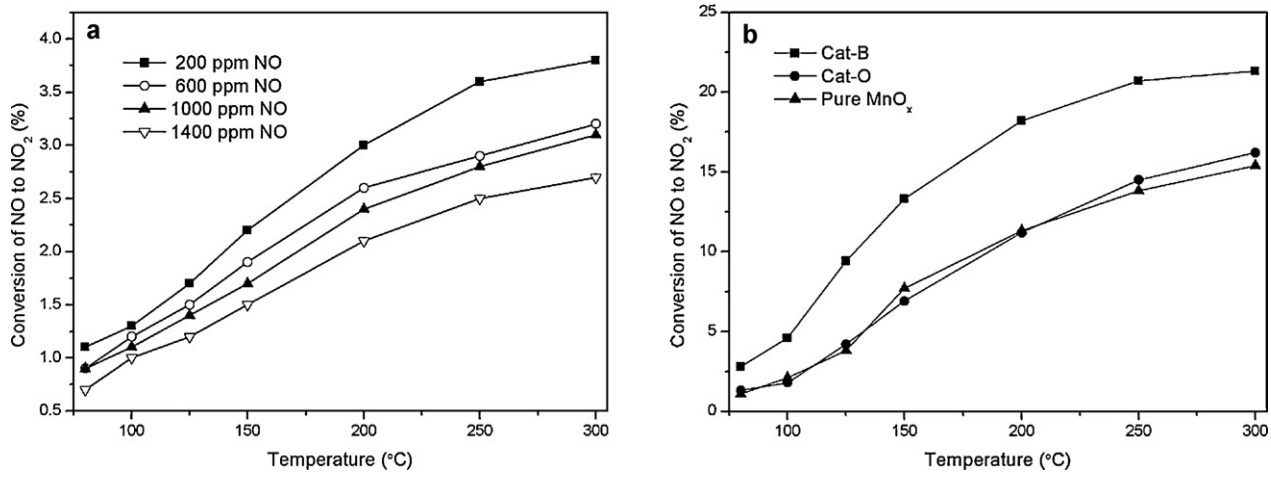

Fig. 3. (a) Oxidation activity of NO to NO_2 by O_2 in the absence of catalyst. Reaction conditions: 200 ppm, 600 ppm, 1000 ppm or 1400 ppm NO, 5% O_2 and Ar balance, GHSV = 10,000 h^{-1}. (b) Oxidation activity of NO to NO_2 by O_2 over MnO_x, MnO_x/TiO_2 and Cat-B. Reaction conditions: 1000 ppm NO, 5% O_2 and Ar balance, GHSV = 10,000 h^{-1}.

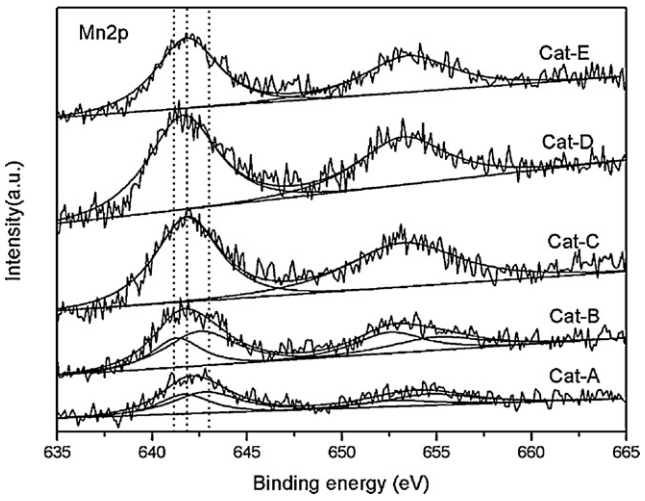

Fig. 4. Mn 2p XPS spectras of MnO_x/CZA catalysts.

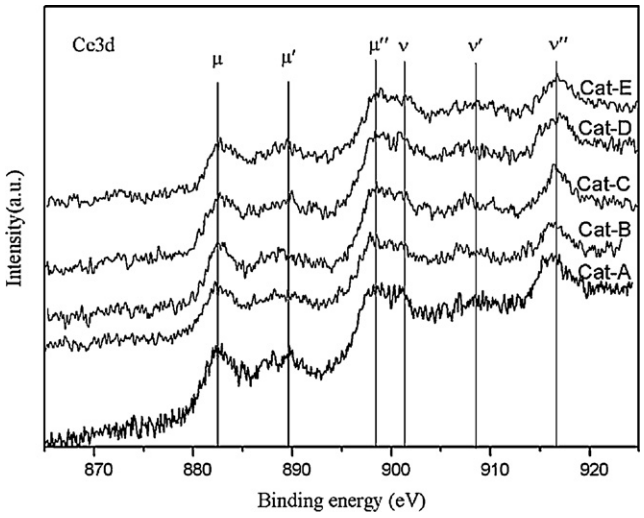

Fig. 5. Ce 3d XPS spectras of MnO_x/CZA catalysts.

observed with the increasing of Mn loading. It can be seen that there are two groups of Mn 2p fitting peaks in Cat-A and Cat-B, which can be explained due the presence of different oxidation states of Mn. The main peaks of the Mn $2p_{3/2}$ level at higher BE value of 642.8 eV for Cat-A and 642.5 eV for Cat-B are attributed to the Mn^{4+} species of MnO_2 [19,20]. The main peak at lower BE value of 641.7 eV in Cat-A is attributed to the Mn^{3+} species of Mn_2O_3 [19–21]. For Cat-B, the lower BE value peak is shifted to 641.3 eV, which can be attributed to a mixed-valence of Mn^{3+} and Mn^{2+} cations within the surface of this catalyst. On the other hand, the BE value here also can be attributed to the Mn_3O_4 species [19–22]. The BE values of MnO and Mn_2O_3 are very close to each other, which causes difficulty in unambiguous identification of the oxidation state [19,20,22]. The Mn $2p_{3/2}$ peaks in Cat-C, Cat-D and Cat-E have only one electronic binding energy peak, which is locate at 641.8, 641.6 and 641.8 eV, respectively. It is obvious that the Mn $2p_{3/2}$ BE values of Cat-C, Cat-D and Cat-E are characteristic of Mn^{3+} species [19,20]. These results illustrates the presence of MnO_2 as a major phase along with Mn_3O_4 as the minor phase at lower loadings; but the MnO_2 phase disappears at higher Mn loading.

Fig. 5 shows the Ce 3d XPS spectra of MnO_x/CZA catalysts. It can be seen that Ce 3d spectras are very complicated, which can be resolved into six components. The series of peaks denoted by "u" and "v" represent the Ce $3d_{5/2}$ and the Ce $3d_{3/2}$ states contribution, respectively. From these peaks, Ce^{4+} oxidation state is predominant, and Ce^{3+} oxidation state is indistinct identification through the Ce 3d spectra [19,23,24]. The peaks of u and u′ can be assigned to a mixing of $3d^94f^2$ ($O\ 2p^4$) and $3d^94f^1$ ($O\ 2p^5$) Ce^{4+} final states, and u″ to the $3d^94f^0$ ($O\ 2p^6$) Ce^{4+} state. The series of v structures from the Ce $3d_{3/2}$ states can be explained in the same way [24,25]. The u peak of Ce $3d_{5/2}$ is locate at 882.0 eV for pure CeO_2 [19]. As show in Table 2, the u peaks of Ce $3d_{5/2}$ BE of MnO_x/CZA catalysts are apparently higher than that of pure CeO_2. Otherwise, the BE value of u gradually shifts to higher binding energy with the increase of manganese content. It can be seen that the addition of MnO_x changes the surface chemical surrounding of Ce atom, and this indicates that strong interaction exists between Ce and other atoms.

As shown in Table 2, it can be observed that the increasing manganese content increases the molar percentage of Mn on the surface of catalyst until the manganese loading reached 20%, while the molar percentage of Ce decrease. However, when the manganese loading reaches 30%, the surface molar percentage of Mn decreases, and that of Ce increases. Furthermore, the Mn^{4+}/Mn 2p molar ratio can be taken as a measure of the main active phase of manganese oxide on the catalyst surface (see Table 2). As can be noted, the molar ratio of Mn^{4+}/Mn 2p is 58.8% in Cat-A and 62.9% in Cat-B, which indicates that the support surface is mainly covered by MnO_2 at lower manganese loadings ($\leq$10%). It is well known that the detection depth of XPS analysis is only 2 nm. Therefore, we suggest that the crystalline manganese oxides may agglomerate to nanometer particle with a size larger than 2 nm, and they may also insert into the pore structure of CZA. On the other hand, the excess Mn atoms may migrate into the bulk phase of Cat-E. All of the above suggestions cause the site of manganese exceeding the detection depth of XPS technique. It can be concluded that the Mn_3O_4 phase detected by XRD in Cat-C, Cat-D and Cat-E exceed the detection depth of XPS testing.

Imamura et al. and Ding et al. suggested that a synergistic effect existed between the manganese and cerium oxides when simultaneous existing of Mn_2O_3 and CeO_2 [26,27]. Kapteijn et al. [28] suggested that the activity and selectivity of manganese oxide were obviously influenced by the oxidation state and the degree of crystallinity. The Mn_2O_3 exhibited the highest selectivity for N_2 while the MnO_2 exhibited the highest activity. Therefore, it can be concluded that the existent synergistic effect between the manganese and cerium oxides may be a main contribution to the SCR activity

Table 2
Binding energy, surface molar percentage and relative area ratio of different manganese species determined from XPS and TPR.

Sample	Binding energy (eV)		Molar percentage		Mn^{4+}/Mn (XPS, %)	Area ratio of $Mn^{4+} \rightarrow Mn^{3+}$ and $Mn^{3+} \rightarrow Mn^{2+}$ (TPR)
	Mn $2p_{3/2}$	Ce $3d_{5/2}$	Mn (%)	Ce (%)		
Cat-A	641.7; 642.8	882.5	1.89	4.81	58.8	4:2
Cat-B	641.3; 642.5	882.6	2.91	3.44	62.9	5:2
Cat-C	641.8	882.7	3.44	2.73	0	3:2
Cat-D	641.6	882.9	3.82	2.77	0	2:2
Cat-E	641.8	882.9	3.57	3.30	0	3:2

over MnO_x/CZA catalysts, and the various oxidation state of Mn in Cat-B may be another contribution to the excellent SCR activity.

3.5. H_2-TPR study

The H_2-TPR was used in the present study to investigate the oxidation states of CZA support and MnO_x/CZA catalysts. The Gaussian fitting results of H_2-TPR are shown in Fig. 6, the CZA support shows a main reduction peak with the maximum at 508 °C in the range of 100–700 °C, indicating the reduction of surface Ce^{4+} to Ce^{3+} [29]. A very small shoulder is also observed in CZA around 420 °C, which is assigned to the reduction of surface absorbed oxygen species. After MnO_x is supported on CZA, the reduction peaks of samples are obviously broadened. This suggests that the reducible manganese species exists in a mixed-valence such as MnO_2, Mn_2O_3 or Mn_3O_4, which is consistent with the results of XPS and XRD. The TPR profiles of Cat-A, Cat-B and Cat-C samples exhibit three reduction peaks. The reduction peak around 360 °C is attributed to the reduction of MnO_2 to Mn_2O_3 and the reduction of surface absorbed oxygen species, and the reduction peaks at higher temperature of 400–700 °C are assigned to the reduction of $Mn_2O_3 \rightarrow MnO$ and the reduction of bulk phase absorbed oxygen species [30–32]. This reduction process has two types. The reduction peak around 450 °C can be regarded as the reduction of Mn_2O_3 to Mn_3O_4 [30–32]. The reduction peak around 480–600 °C should be assigned to the reduction of both Mn_3O_4 to MnO and reducible surface CeO_2 to Ce_2O_3 [30–33]. For Cat-D and Cat-E, there are two hydrogen consumption peaks in the range of 100–700 °C, the reduction peak around 380 °C belongs to the reduction of MnO_2 to Mn_3O_4, whereas the higher temperature peak represented the reduction of $Mn_3O_4 \rightarrow MnO$, $Mn_2O_3 \rightarrow MnO$ and easily reducible surface CeO_2 to Ce_2O_3 [30,31,34]. This indicates that the increased manganese loading may induce the reduction of MnO_2 to MnO from three steps to two steps.

Fig. 6 indicates that the reduction temperature of MnO_2 to Mn_2O_3 over Cat-B is lower than that of the other catalysts, which illustrates that the MnO_x on Cat-B is more active than the other catalysts. This indicates that the lower reduction temperature represents the higher dispersion of MnO_x over the surface of CZA. When the manganese loading exceeds 10%, the reduction temperature of MnO_2 gradually shifts towards higher temperature with

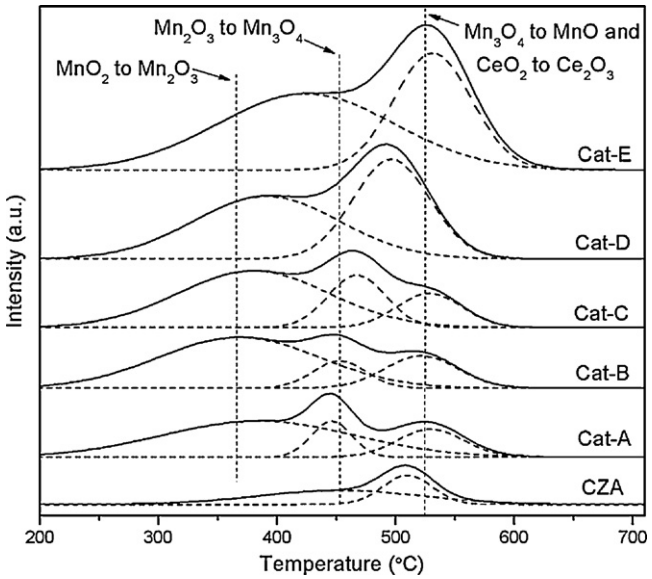

Fig. 6. The H_2-TPR profiles of CZA and MnO_x/CZA catalysts.

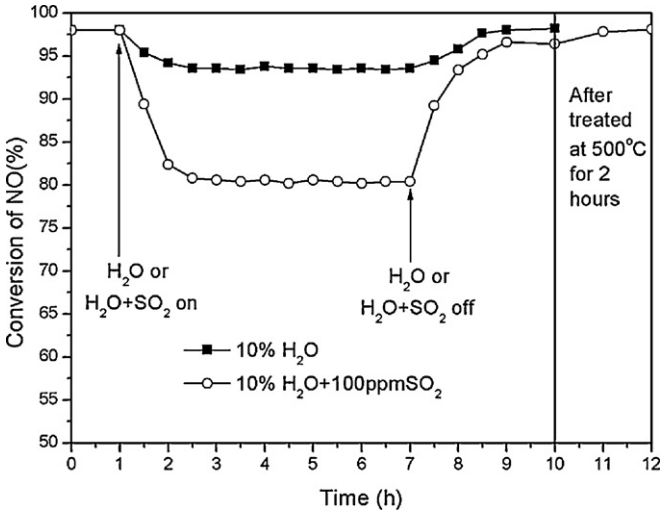

Fig. 7. The effects of H_2O and SO_2 on the SCR activity of Cat-B catalyst. Reaction conditions: 416 ml min^{-1} total flow rate, 1000 ppm NO, 1000 ppm NH_3, 5% O_2, 10% H_2O (when used), 100 ppm SO_2 (when used) and Ar balance, 200 °C, GHSV = 10,000 h^{-1}.

increasing of manganese content. It is obvious that the finely dispersed manganese oxide decreases with the increase of manganese loading. But for Cat-A, there is only a week shoulder peak for the reduction of highly dispersed surface MnO_x, which indicates that some free surface sites are not occupied by MnO_x species on the surface of CZA. The result is also supported by the XRD results mentioned in Fig. 1. When the manganese content reach 20%, the increased concentration of crystalline Mn_3O_4 species in catalysts results in an enhanced intensity of the hydrogen consumption peak in the range of 450–550 °C.

As shown in Table 2, the relative ratios of the reduction process of $MnO_2 \rightarrow Mn_2O_3$ and $Mn_2O_3 \rightarrow MnO$ are calculated from the H_2 consumption during the TPR process. It can be seen that the majority of manganese species is MnO_2 for all catalysts. The area ratio of the two step reduction process $MnO_2 \rightarrow Mn_2O_3 \rightarrow MnO$ is calculated to be nearly 5:2 for Cat-B, which implied that the percentage of MnO_2 species is the largest in Cat-B. Herein, the intermediate manganese species in the reduction of $MnO_2 \rightarrow Mn_2O_3$ had similar oxidation state as that in Mn_2O_3. This clearly demonstrates that the MnO_2 species is the mainly active species in MnO_x/CZA catalyst.

From the XRD results, it can be seen that no visible MnO_2 diffraction peaks are observed in MnO_x/CZA catalysts. But from the XPS analysis, the oxidation state of MnO_2 is detected only in Cat-A and Cat-B. The TPR results conclude that most of the manganese species might have stabilized as Mn^{4+} oxidation state on CZA. Furthermore, the activity results showed that the SCR activity of Cat-B is the best. The appearance of Mn_2O_3 and Mn_3O_4 crystal on Cat-C, Cat-D and Cat-E decreases the SCR activity, but the activity is still good. We suggest that MnO_2, Mn_2O_3 and Mn_3O_4 are all active in NH_3-SCR reaction, but MnO_2 is more active than that of Mn_2O_3 and Mn_3O_4 [11,28].

3.6. Effect of SO_2 and H_2O

Flue gases always contain small concentrations of SO_2 and some concentrations of H_2O, even after desulphurization. It has been suggested that the coexistence of SO_2 and H_2O has a serious poisoning effect on SCR activity at low temperature. Therefore, it is significant to investigate the effect of H_2O and SO_2 on low-temperature SCR reaction. The effect of H_2O and $SO_2 + H_2O$ on SCR activity over Cat-B catalyst is illustrated in Fig. 7. Before introducing 10% H_2O or 100 ppm

SO_2 + 10% H_2O, the SCR reaction has stabilized for 1 h at 200 °C.

As shown in Fig. 7, when 10% H_2O was added to the reaction gases, the NO conversion slightly decreases to about 93% from its original level, and then NO conversion almost stabilizes. After the removal of the water supply, the SCR activity increases and restores to its original level after 1.5 h. When 100 ppm SO_2 and 10% H_2O were added to the reactants at 200 °C with a space velocity of 10,000 h^{-1}, the NO conversion rapidly decreases to 80.4% from 98% in 1.5 h, and then nearly stabilizes. After turning off the SO_2 and H_2O, the activity quickly restores to 96.4%. When the catalyst was heated for 2 h in Ar at 500 °C, the activity quickly restores to its initial level. This indicates that the Cat-B is resistant to water vapor and the mixture of H_2O and SO_2 at 200 °C. The decreased activity in the process is mainly caused by the competing adsorption of H_2O, SO_2 and reaction gases on the catalyst. It is clear that a small portion of tightly adsorbed SO_2, the formed sulfates, and the ammonium sulfates on the catalyst surface occupy the active sites of catalyst, which consequently lead to the decrease of SCR activity [35,36]. After a heating treatment, the adsorbed SO_2 desorbs from the catalyst surface and the formed sulfates and ammonium sulfates decompose into SO_x (SO_2 or SO_3) and NH_3, which is taken away by the blowing gas, so the SCR activity restores to its original level.

4. Conclusions

The present work has shown that the MnO_x/CZA monolithic catalysts are more active than pure manganese oxide and MnO_x/TiO_2 catalysts for low-temperature SCR of NO with NH_3 in the presence of excess oxygen. The increases of manganese loading enhances the NO conversion of MnO_x/CZA catalysts until manganese content up to 10%, and a further increase of manganese content decreases the SCR activity. The MnO_x/CZA catalyst with 10% manganese loading presents the best catalytic activity for NO reduction. At higher manganese loading, the decreased activities of catalysts are caused by the formation of crystalline manganese oxides such as Mn_3O_4 and Mn_2O_3. The superior SCR activity of MnO_x/CZA catalyst with 10% manganese loading is due to the highly dispersed MnO_x over CZA and the excellent oxidation activity of NO to NO_2. At 10% manganese loading, the manganese oxides species presents various oxidation states such as MnO_2, Mn_3O_4 and MnO, and all of the manganese oxides species are highly dispersed or amorphous. The finely dispersed MnO_2 species is easily reduced at lower temperature in H_2-TPR. This catalyst is also resistant to water vapor and the mixture of H_2O and SO_2.

Acknowledgements

We gratefully acknowledge the financial support from the Program of National Natural Science Foundation of China (NSFC. 20333030 and 20773090). We also thank Professor Jumu Zhu and Mr. Chuan Xin for XRD and XPS measurements, respectively.

References

[1] J. Kaspar, P. Fornasiero, N. Hickey, Catal. Today 77 (2003) 419–449.
[2] S. Djerad, L. Tifouti, M. Crocoll, W. Weisweiler, J. Mol. Catal. A 208 (2004) 257–265.
[3] S.T. Choo, S.D. Yim, I.S. Nam, S.W. Ham, J.B. Lee, Appl. Catal. B: Environ. 44 (2003) 237–252.
[4] M. Kang, E.D. Park, J.M. Kim, J.E. Yie, Catal. Today 111 (2006) 236–241.
[5] Z.B. Wu, B.Q. Jiang, Y. Liu, Appl. Catal. B: Environ. 79 (2008) 347–355.
[6] J.H. Huang, Z.Q. Tong, Y. Huang, J.F. Zhang, Appl. Catal. B: Environ. 78 (2008) 309–314.
[7] P.G. Smirniotis, P.M. Sreekanth, D.A. Peña, R.G. Jenkins, Ind. Eng. Chem. Res. 45 (2006) 6436–6443.
[8] X.L. Tang, J.M. Hao, H.H. Yi, J.H. Li, Catal. Today 126 (2007) 406–411.
[9] T. Valdés-Solís, G. Marbán, A.B. Fuertes, Catal. Today 69 (2001) 259–264.
[10] W.S. Kijlstra, D.S. Brands, E.K. Poels, A. Bliek, J. Catal. 171 (1997) 208–218.
[11] G. Qi, R.T. Yang, R. Chang, Appl. Catal. B: Environ. 51 (2004) 93–106.
[12] G. Qi, R.T. Yang, J. Phys. Chem. B 108 (2004) 15738–15747.
[13] A. Morikawa, T. Suzuki, T. Kanazawa, K. Kikuta, A. Suda, H. Shinjo, Appl. Catal. B: Environ. 78 (2008) 210–221.
[14] J. Wang, J. Wen, M.Q. Shen, J. Phys. Chem. C 112 (2008) 5113–5122.
[15] T. Suzuki, A. Morikawa, A. Suda, H. Sobukawa, M. Sugiura, SAE, 2003-01-0811.
[16] H. Choi, S. Ham, I. Nam, Y. Kim, Ind. Eng. Chem. Res. 35 (1996) 106.
[17] M. Koebel, G. Madia, M. Elsener, Catal. Today 73 (2002) 239–247.
[18] G. Qi, R.T. Yang, Appl. Catal. B: Environ. 44 (2003) 217–225.
[19] C.D. Wagner, W.M. Riggs, L.E. Davis, J.F. Moulder, G.E. Muilenberg, Handbook of X-ray Photoelectron Spectroscopy, Perkin-Elmer Corporation, Eden Prairie, MN, 1979.
[20] A.S. Reddy, C.S. Gopinath, S. Chilukuri, J. Catal. 243 (2006) 278–291.
[21] F. Li, L. Zhang, D.G. Evans, X. Duan, Colloids Surf. A 244 (2004) 169–177.
[22] B.J. Tan, K.J. Klabunde, P.M.A. Sherwood, J. Am. Chem. Soc. 113 (1991) 855–861.
[23] P. Larsson, A. Andersson, J. Catal. 179 (1998) 72–89.
[24] S. Yang, W. Zhu, Z. Jiang, Z. Chen, J. Wang, Appl. Surf. Sci. 252 (2006) 8499–8505.
[25] D.I. Kondarides, X.E. Verykios, J. Catal. 174 (1998) 52–64.
[26] S. Imamura, A. Dol, S. Ishido, Ind. Eng. Chem. Prod. Res. Dev. 24 (1985) 75.
[27] Z.Y. Ding, L. Li, D. Wade, E.F. Gloyna, Ind. Eng. Chem. Res. 37 (1998) 1707.
[28] F. Kapteijn, L. Singoredjo, A. Andreini, J.A. Moulijn, Appl. Catal. B: Environ. 3 (1994) 173.
[29] H.Q. Zhu, Z.F. Qin, W.Z. Shan, W.J. Shen, J.G. Wang, J. Catal. 225 (2004) 267–277.
[30] Y. Liu, M. Luo, Z. Wei, Q. Xin, P. Ying, C. Li, Appl. Catal. B: Environ. 29 (2001) 61–67.
[31] N. Li, A.Q. Wang, Z.M. Liu, X.D. Wang, M.Y. Zheng, Y.Q. Huang, T. Zhang, Appl. Catal. B: Environ. 62 (2006) 292–298.
[32] P.R. Ettireddy, N. Ettireddy, S. Mamedov, P. Boolchand, P.G. Smirniotis, Appl. Catal. B: Environ. 76 (2007) 123–134.
[33] X.D. Wu, Q. Liang, D. Weng, J. Fan, R. Ran, Catal. Today 126 (2007) 430–435.
[34] V.P. Santos, M.F.R. Pereira, J.J.M. Órfão, J.L. Figueiredo, Appl. Catal. B: Environ. 99 (2010) 353–363.
[35] T.S. Park, S.K. Jeong, S.H. Hong, S.C. Hong, Ind. Eng. Chem. Res. 40 (2001) 4491–4495.
[36] X.L. Tang, J.M. Hao, W.G. Xu, J.H. Li, Catal. Commun. 8 (2007) 329–334.